Biochemical and Biophysical Research Communications 463 (2015) 762–767

Contents lists available at ScienceDirect

Biochemical and Biophysical Research Communications

journal homepage: www.elsevier.com/locate/ybbrc

Crystal structure of syndesmos and its interaction with Syndecan-4 proteoglycan

Heeyoun Kim [a], Jiho Yoo [b], Inhwan Lee [a], Ying Jin Kang [b], Hyun-Soo Cho [b, **], Weontae Lee [a, *]

[a] Department of Biochemistry, College of Life Science and Biotechnology, Yonsei University, Seoul, 120-749, South Korea
[b] Department of Systems Biology, College of Life Science and Biotechnology, Yonsei University, Seoul, 120-749, South Korea

ARTICLE INFO

Article history:
Received 22 May 2015
Accepted 2 June 2015
Available online 19 June 2015

Keywords:
Syndesmos
Nudix hydrolase
Syndecan-4
X-ray crystallography
NMR spectroscopy

ABSTRACT

Syndesmos, nucleoside diphosphate linked moiety X (nudix)-type motif 16-like 1 (Nudt16l1), is evolutionarily divergent from the Nudt16 family. Syndesmos, which is co-localized with syndecan-4 cytoplasmic domain ($Syn4^{cyto}$) in focal contacts, interacts with various cell adhesion adaptor proteins to control cell signaling. We determined the X-ray crystal structure of syndesmos; it is composed of seven α-helices and seven β-strands. Although syndesmos has a molecular topology similar to that of nudix hydrolase proteins, the structure of the nudix motif differs from that of X29. The dimeric interface of syndesmos is composed of α-helix 4, 7 and β-strand 2, 7, which primarily form hydrophobic interactions. The binding interaction between syndesmos and $syn4^{cyto}$ was characterized as a low-affinity interaction (K_d = 62 μM) by surface plasmon resonance (SPR) and nuclear magnetic resonance (NMR). The NMR resonances of Lys (177, 178, 179), Gly182, and Ser183 in the C1 region and Lys193 and Lys194 in the V region of syndecan-4 are perturbed upon syndesmos binding. Our results provide structural insight into the molecular function of syndesmos in the regulation of cell signaling via binding to syndecan-4.

1. Introduction

Syndesmos is a member of the nudix hydrolase family that possesses pyrophosphate hydrolysis activity; it has high sequence homology with Nudt16 [1–3]. The sequence similarity between syndesmos and Nudt16 implies that syndesmos is a paralogous protein resulting from gene duplication, which occurred in the tetrapod lineage near the amniote divergence for Nudt16 [3]. Nudt16 contains a common nudix motif, $GX_5EX_7REUXEEXGU$ (U indicates a bulky hydrophobic residue), which coordinates with divalent metals, such as Mn^{2+} or Mg^{2+}, to bind to pyrophosphate [1–5]. Recently, the crystal structure of X29 was reported [6,7]. X29 possesses RNA capping cleavage activity that controls mRNA turnover [4,7–9]. The sequence identity between syndesmos and X29 is 46% (97/211). However, the glutamate residues that coordinate divalent metals are not conserved in syndesmos, suggesting that syndesmos has a different function. Interestingly, syndesmos is expressed in several organs and participates in focal adhesion formation upon binding to the cytoplasmic domain of syndecan-4 ($Syn4^{cyto}$) [10,11]. When syndesmos is overexpressed in cells, cell spreading and cytoskeleton organization are improved, which is confirmed by enhanced formation of filipodia. These results were not affected by serum or media type, but only by cell adhesion complex formation, suggesting that the cellular features caused by syndesmos overexpression are closely related to the interaction with $Syn4^{cyto}$ containing a cell adhesion complex [10]. The syndecan protein family, which consists of syndecan-1, -2, -3, and -4, is comprised of proteins that are well-known single transmembrane proteins for cell adhesion, also known as heparan sulfate proteoglycans [10,12,13]. Syndecan participates in formation of the cell adhesion complex and controls cell growth, proliferation, survival, and migration. $Syn4^{cyto}$ is expressed in a wide variety of cells and interacts with cytoskeleton. Through the cytoplasmic domain, syndecan-4 controls the activity of protein kinase C_α (PKC_α), which transfers cell signals from the extracellular matrix [13,14]. $Syn4^{cyto}$

* Corresponding author. Department of Biochemistry, College of Life Science and Biotechnology, Yonsei University, 50 Yonsei-ro, Seodaemun-gu, Seoul, 120-749, South Korea.
** Corresponding author. Department of Systems Biology, College of Life Science and Biotechnology, Yonsei University, 50 Yonsei-ro, Seodaemun-gu, Seoul, 120-749, South Korea.
E-mail addresses: hscho8@yonsei.ac.kr (H.-S. Cho), wlee@spin.yonsei.ac.kr (W. Lee).

http://dx.doi.org/10.1016/j.bbrc.2015.06.010
0006-291X/

consists of three individual regions, the conserved 1 region (C1 region), the variable region (V region), and the conserved 2 region (C2 region) [15]. Each region interacts with several proteins: the C2 region interacts with PDZ domain-containing proteins and the V region interacts with phosphatidylinositol 4,5-bisphosphate (PIP2) and syndesmos [16–20]. Recently, it has been reported that syndesmos interacts with Syn4^{cyto} and focal adhesion complex proteins, such as paxillin and hic-5, suggesting that the cellular function of syndesmos has a direct relationship with Syn4^{cyto} and focal adhesions [10,11]. To identify the molecular mechanism and functions of the syndesmos/Syn4^{cyto} complex, we determined the crystal structure of mouse syndesmos and performed biochemical experiments using SEC, SPR, and NMR titrations.

2. Materials and methods

2.1. Cloning, protein purification, and sample preparation

cDNA encoding Syndesmos and Syn4^{cyto} were amplified by PCR using synthetic oligonucleotides as primers and were subcloned into the *Escherichia coli* expression vector pET32a (Amersham Biosciences). Both plasmids were transformed into *E. coli* strain BL21(DE3) for expression, and grown in either Luria–Bertani (LB) or M9 minimal media. Cells were cultured at 37 °C until they reached an OD_{600} of 0.6, 1 mM IPTG was added, and cells were cultured further for 15 h at 25 °C. Subsequently, the cells were harvested by centrifugation and stored at −80 °C. Harvested TRX-$(His)_6$ tag-fusion proteins were purified by immobilized metal affinity chromatography (IMAC) using a Ni-NTA column (Amersham Pharmacia), and the TRX-$(His)_6$ tag was cleaved by incubation with tobacco etch virus protease for 2–3 h at 25 °C. The purified proteins were then subjected to size exclusion chromatography using a HiLoad Superdex 75 prep grade column (Amersham Pharmacia). Syn4^{cyto} was purified to a high degree of purity using a reversed-phase HPLC column (C18, 300 × 3.9 mm, Waters, USA) with a Delta 600 HPLC system (Waters, USA). For X-ray crystallography, syndesmos was purified as described above and dialyzed with final buffer containing 10 mM HEPES (pH 7.0), 100 mM NaCl, and 2 mM DTT. For NMR experiments, Syn4^{cyto} protein was labeled with ^{15}N or $^{13}C/^{15}N$ by culturing in M9 minimal medium containing $^{15}NH_4Cl$ (Cambridge Isotope Laboratories Inc.) and/or U-$^{13}C_6$-glucose (Cambridge Isotope Laboratories Inc.). The final buffer contained 10 mM HEPES (pH 7.0), 150 mM NaCl, and 0.01% NaN_3.

2.2. X-ray data collection and crystal structure determination

Syndesmos crystals were grown under 0.2 M Li sulfate, 0.1 M Bis-Tris (pH 5.5), 25% m/w PEG3350, and 20% glycerol was added as a cryo-protectant. Diffraction data with resolution of 2.01 Å were collected on beam line 5C/7A at the Pohang Accelerator Laboratory, Korea. The data set was processed and scaled using DENZO and SCALEPACK in the HKL2000 package [21,22]. The crystal of syndesmos belongs to space group P_12_1, with a unit-cell dimension of a = 45.318 Å, b = 68.701 Å, and c = 66.171 Å. Assuming that two molecules may form an asymmetric unit, the Matthew's coefficient (Vm) was calculated to be 2.1 Å 3/Da, which corresponds to a solvent content of 40.8%. The initial phase was obtained by molecular replacement using the CCP4 version of MOLREP [23,24], and the structure of sX29 (PDB: 3COU) was used as a search model. Coot [25] and PHENIX [26] were used for model building and refinement. The X-ray structure of mouse syndesmos was deposited under PDB ID 4ZG0; all parameters are shown in Table 1. The following servers were used for sequence and structural analysis: BLAST (http://blast.ncbi.nlm.nih.gov/Blast.cgi), DALI (http://ekhidna.biocenter.helsink.fi/dali-server), and PDBePISA (Protein Interfaces, Surface, and Assemblies) [27,28].

Table 1
Data collection and refinement statistics.

	Syndesmos
Data collection	
Space group	$P2_1$
Cell dimensions	
a, b, c (Å)	45.318 68.701 66.191
α, β, γ (°)	90.00 103.93 90.00
Resolution (Å)	50.00–2.00 (2.07-2.00)*
R_{sym} or R_{merge}	0.072 (0.155)
$I/\sigma(I)$	34.79 (7.62)
Completeness (%)	96.01 (89.3)
Redundancy	4.1 (3.0)
Refinement	
Resolution	37.044 (2.006)
No. reflections	25424
R_{work}/R_{free}	0.1778/0.2254
N.o atoms	
Protein	3047
Water	259
R.m.s deviations	
Bond lengths	0.008
Bond angles	1.087

*Values in parentheses are for highest-resolution shell.

2.3. Affinity measurements by SPR

Surface plasmon resonance (SPR) was performed at 25 °C using a BIAcore 2000 instrument (BIAcore, GE Healthcare). A total of 200–300 RU (response units) was immobilized on a streptavidin-coated SA chip with a biotinylated synthetic peptide corresponding to Syn4^{cyto}. The SA chip contained four flow cells; one flow cell was activated and blocked in the same way (without Syn4^{cyto}), and the other cell was used as a reference for non-specific binding. Syndesmos (analyte) was perfused over Syn4^{cyto} in running buffer (10 mM HEPES [pH 7.0], 100 mM NaCl, and 2 mM DTT) with a flow rate of 30 μl/min. The surface of the sensor chip was regenerated by injecting a buffer containing 1 M NaCl and 0.05 M NaOH for 1 min [16]. The dissociation constant (Kd) was calculated using the software BIAevaluation v. 3.1 and the buffer effects were subtracted from each curve.

2.4. NMR titration experiments

A series of two-dimensional (2D) [$^{15}N–^1H$]–HSQC spectra have been collected on uniformly ^{15}N-labeled Syn4^{cyto} (0.5 mM) in the presence of different amounts of syndesmos, with molar ratios of 1:0, 1:0.5, and 1:1 (Syn4^{cyto}: syndesmos). Samples were prepared in 10 mM HEPES (pH 7.0), 100 mM NaCl, 2 mM DTT, and 0.01% NaN_3. NMR resonances for Syn4^{cyto} were assigned previously, using three-dimensional (3D) HNCACB, CBCA(CO)NH, HNCA, and HNCO data [29–32]. All NMR experiments were performed on Bruker 500 MHz and 800 MHz spectrometers equipped with a *z*-shielded gradient triple-resonance cryoprobe. All NMR data were processed using the XWINNMR program and the software NMRpipe/NMRDraw [33].

3. Results and discussion

3.1. X-ray crystal structure of syndesmos

Syndesmos consists of 211 amino acids, and it is highly homologous with proteins in the Nudt16 family. The crystal structure of syndesmos has been determined at a resolution of 2.01 Å by

molecular replacement (Table 1). The final structure shows an R_{cryst} of 17.8% and a R_{free} of 22.5%. Two syndesmos molecules were observed to form an asymmetric unit, which was revealed to be a dimer. The overall molecular topology and secondary structures are shown in Fig. 1A and B, respectively. Syndesmos is composed of seven α-helices and seven β-strands; α1 (14–17), α2 (74–82), α3 (93–95), α4 (119–129), α5 (157–161), α6 (167–179), α7 (185–203), β1 (25–35), β2 (48–55), β3 (58–61), β4 (64–66), β5 (97–101), β6 (108–116), and β7 (139–144). Specific residues in the secondary structure of the dimeric interface are marked with yellow asterisks; in particular, α4, α7, β2, and β7 are involved in the dimeric interface (Fig. 1B). Hydrophobic interactions, hydrogen bonds, and salt bridges all contribute to dimer formation of syndesmos. Dimerization occurs mainly by hydrophobic interactions via an extensive hydrophobic interface (Fig. 2A), and the major contact area spans 1522.0 Å (14.4%) of the surface area of each monomer, with a calculated solvation free energy gained upon formation of the interface ($\Delta^{i}G$) of −21.5 kcal/mol, as determined by PISA [27,28]. To confirm whether dimerization was an artifact of crystallization, gel filtration analysis was performed (data not shown). The results

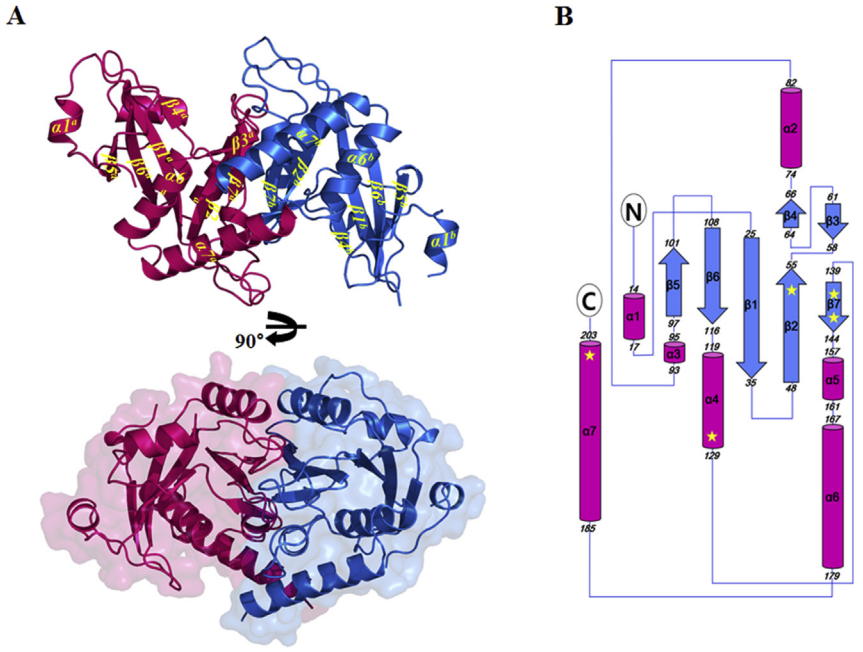

Fig. 1. X-ray crystal structure of syndesmos. (A) The X-ray crystal structure of syndesmos, represented by a ribbon diagram. The structure was visualized using the Pymol program. Seven α-helices and seven β-strands are represented. (B) Schematic diagram of the molecular topology of syndesmos. α-Helices and β-strands are shown with cylinders and arrows, respectively, with residue numbers shown alongside. Specific residues involved in the dimeric interface are represented by yellow asterisks. (For interpretation of the colors used in this figure legend, the reader is referred to the web version of this article.)

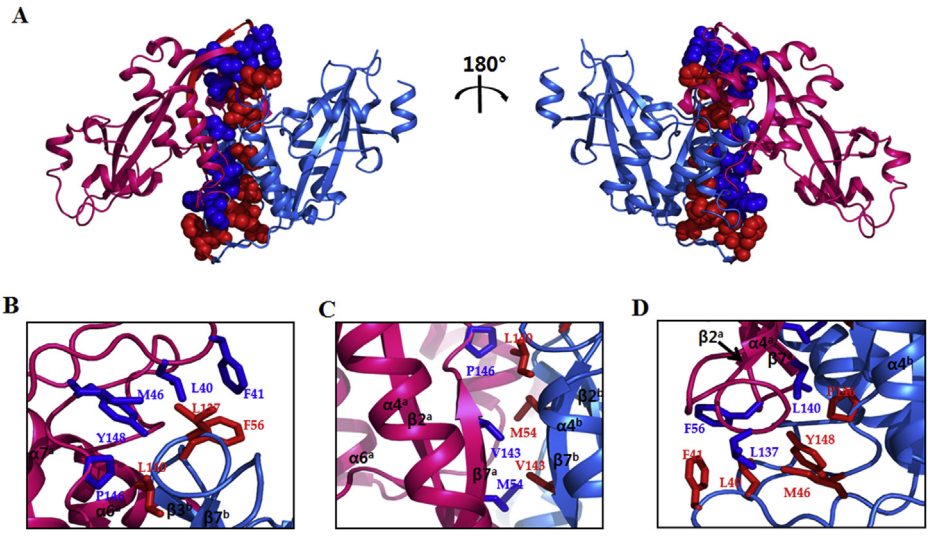

Fig. 2. Dimeric interface of syndesmos and the hydrophobic interactions involved. (A) Dimeric interface with a hydrophobic patch. The structure was rotated by 180° on the y-axis. The hydrophobic residues are represented using a sphere model. The overall structure is maintained by these hydrophobic interactions. (B–D) Not all hydrogen atoms are represented. Detailed views of hydrophobic side-chain connectivity are shown. Hydrophobic residues were located in β2, β7, α4, and α7. L40, F41, M46, F56, L140, and V143 in β2, β7, and the loops were the main contributors to the hydrophobic interactions. These are represented using stick models.

showed that syndesmos exists as a dimer in solution, consistent with the crystal packing analysis. Syndesmos dimerizes via α4-α4, α7-α7, β2-loop, β7-loop, and β7-β7 hydrophobic interactions. The hydrophobic core is constituted by residues Leu40, Phe41, Met46, Met54, Phe56, Leu137, Leu140, Val143, Pro146, and Tyr148 in β2-loop, β7-loop, and β7-β7; these residues stabilize and maintain the integrity of the overall tertiary structure (Fig. 2B–D). The dimerization of syndesmos is further stabilized by peripheral interactions primarily between hydrophobic residues (Ile127, Val130, and Leu203). In addition, formation of hydrogen bonds (Phe56-Y148, Asp57-Gly156, Gly58-Asn159, His123-Val130, Glu126-His135, Lue140-Arg144, and Asn163-Ala164) and salt bridges (Glu126-His135) among these residues also support the dimeric structure. The distribution of these hydrophobic amino acids in the dimeric interface shows that they have a major effect on determining the tertiary structure via hydrophobic interactions between the two monomers, resulting in formation of the compact dimer of syndesmos.

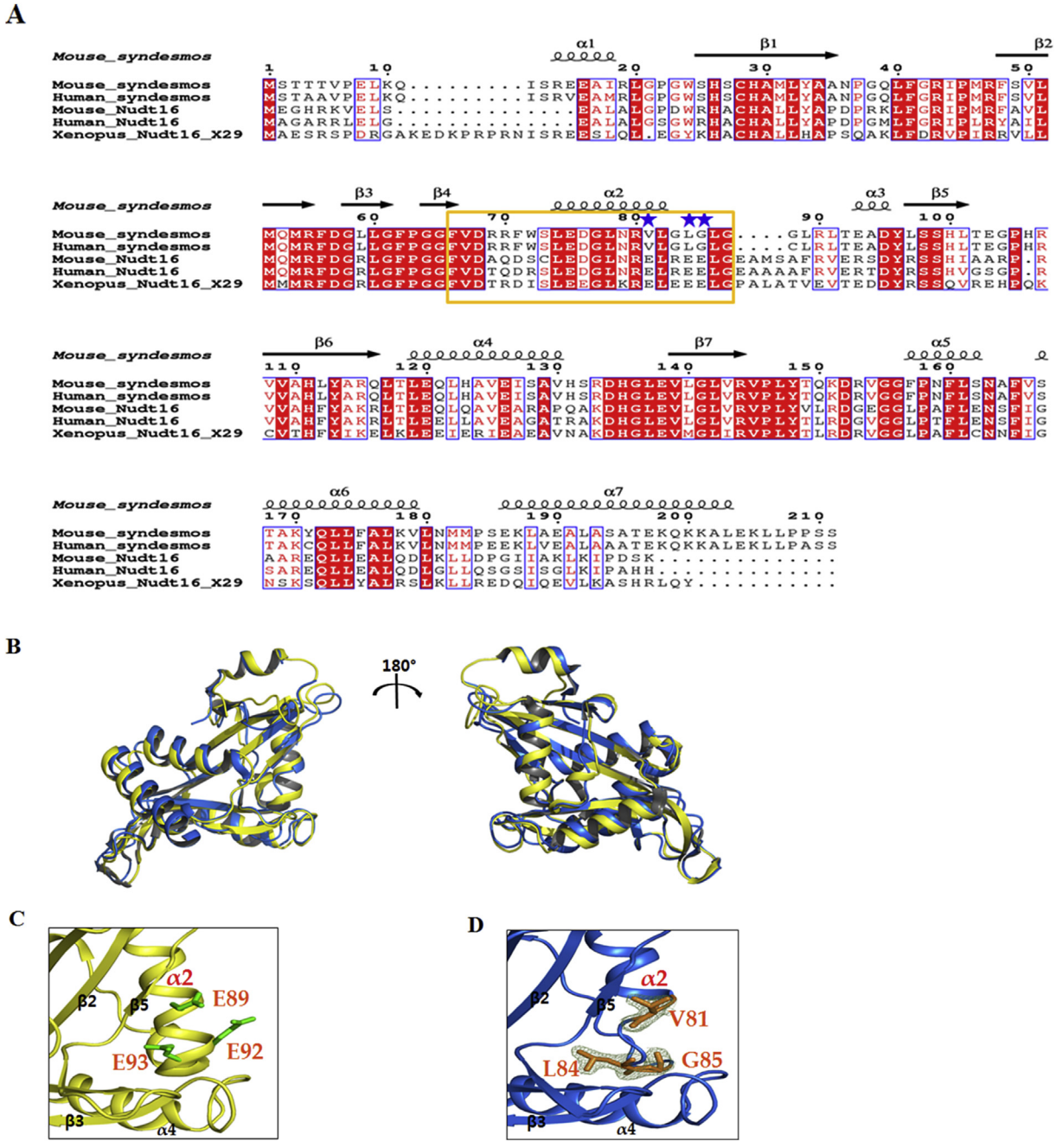

Fig. 3. Sequence alignment of the nudix hydrolase family proteins and structural comparison of syndesmos and Nudt16. (A) Multiple sequence alignment of mouse syndesmos, human syndesmos, mouse Nudt16, human Nudt16, and *Xenopus* Nudt16 is displayed. The nudix motif is highly conserved, with the exception of several residues. The sequence alignment was produced using T-COFFEE and rendered using ESPript. (B) Crystal structures of both syndesmos (blue) and X29 (yellow) is displayed with superposition. The root mean square deviation (RMSD) of the backbone atoms between two structures is calculated as a 1.18Å. (C, D) Structures of the nudix motif are shown for both X29 (C) and syndesmos (D). Residues, Glu89, Glu92 and Glu93 of X29 are corresponding to Val81, Leu84 and Gly85 of syndesmos. (For interpretation of the colors used in this figure legend, the reader is referred to the web version of this article.)

3.2. Structural comparison of syndesmos with Nudt16 proteins

We performed multiple sequence alignments among mouse syndesmos, human syndesmos (PDB ID 3KVH), mouse Nudt16, human Nudt16 (PDB ID 3MGM), and *Xenopus* Nudt16 (X29) (PDB ID1U20); the results show that they are highly conserved (Fig. 3A). Nudt16 shows a loop-helix-loop structure in the nudix motif (yellow box) which consists of $GX_5EX_7REUXEEXGU$ (U indicates a bulky hydrophobic residue) in Fig 3A. The sequence identity between syndesmos and X29 (Nudt16, *Xenopus laevis*) was 46% (97/211), and accordingly, high structural similarity was observed when comparing the structure of syndesmos to X29 using the root mean square deviation (RMSD) of backbone atoms <1.18 Å (Fig. 3B). Syndesmos is represented in blue, X29 in yellow. Helix 2 in the nudix motif of X29 contains three glutamate residues that coordinate divalent metals: Glu89, Glu92, and Glu93 [1,2]. In order to bind to pyrophosphate, these three glutamates coordinate with divalent metals, Mn^{2+} or Mg^{2+}. However, syndesmos shows a completely different structure. Helix 2 of syndesmos in the nudix motif is shorter than that of X29 (Fig. 3C, D). In particular, the shortened helix is missing the glutamate residues (Glu92 and Glu93 in X29) that coordinate the two divalent metals; in addition, E89 in X29 was also changed to V81 in syndesmos, suggesting that syndesmos does not possess metal binding activity. Although X29 and syndesmos show high sequence homology and overall structural similarity, differences in the three active site amino acids result in critical functional differences.

3.3. Interaction between syndesmos and $Syn4^{cyto}$

To identify binding affinity between syndesmos and $Syn4^{cyto}$, an SPR experiment was performed. A synthesized biotinylated-$Syn4^{cyto}$ peptide was immobilized on an SA sensor chip and the binding affinity was measured using purified syndesmos as the analyte. The relative response unit (RU) of binding of syndesmos to $Syn4^{cyto}$ was found to correlate to protein concentration (1.625–208 μM), i.e., the RU value increased as the protein concentration increased. The dissociation constant was determined to be $Kd = 6.2 \times 10^{-5}$ M (Fig. 4A). We also performed a series of 2D [$^{15}N-^{1}H$]–HSQC NMR experiments to map the effect of syndesmos-binding events. Based on known NMR data (3D-HNCACB, HNCA, CBCACONH, and HNCO) for $Syn4^{cyto}$ assignments, we titrated syndesmos to $Syn4^{cyto}$ and mapped the binding sites. 2D [$^{15}N-^{1}H$]–HSQC spectra for $Syn4^{cyto}$ alone were overlaid on those of $Syn4^{cyto}$ titrated with syndesmos at molar ratios of 1:0.5 and 1:1 ($Syn4^{cyto}$: syndesmos = 1:0 ([lack], 1:0.5 [blue], 1:1 [red]) (Fig. 4B). To determine the specific location of the protein binding sites, we compared NMR peak intensities for backbone NH groups in 2D [$^{15}N-^{1}H$]–HSQC data for $Syn4^{cyto}$ bound to syndesmos (Fig. 4B, C). The peaks for residues Lys177, Lys179, Gly182, Ser183, and Lys193 disappeared at molar ratios of 1:0.5 and 1:1. The peaks for Lys178, Gly182, and Lys194 also diminished drastically. Although the peaks for Thr197 and Asp198 of $Syn4^{cyto}$ also vanished at a 1:1 M ratio, these residues may not be involved in binding interactions, because the region has already been shown not to interact with syndesmos in pull-down assays [10]. In addition, these residues might be sensitive to changes in the magnetic environment upon titration with syndesmos, leading to line broadening, which is not an interactive event.

The crystal structure of syndesmos shows as a compact dimer stabilized by hydrophobic interactions between monomers. We have shown that the absence of the three key glutamate residues in the nudix motif of syndesmos is responsible for loss of its hydrolase function, despite the high sequence homology between syndesmos and X29 [3]. In X29, the three glutamates in the nudix motif are coordinated with divalent metal ions [3], however, in syndesmos the glutamates are replaced to non-metal binding residues; valine, glycine, and leucine. We found an unwinding of the helix-2 where three glutamates are located. Our observations indicate that the

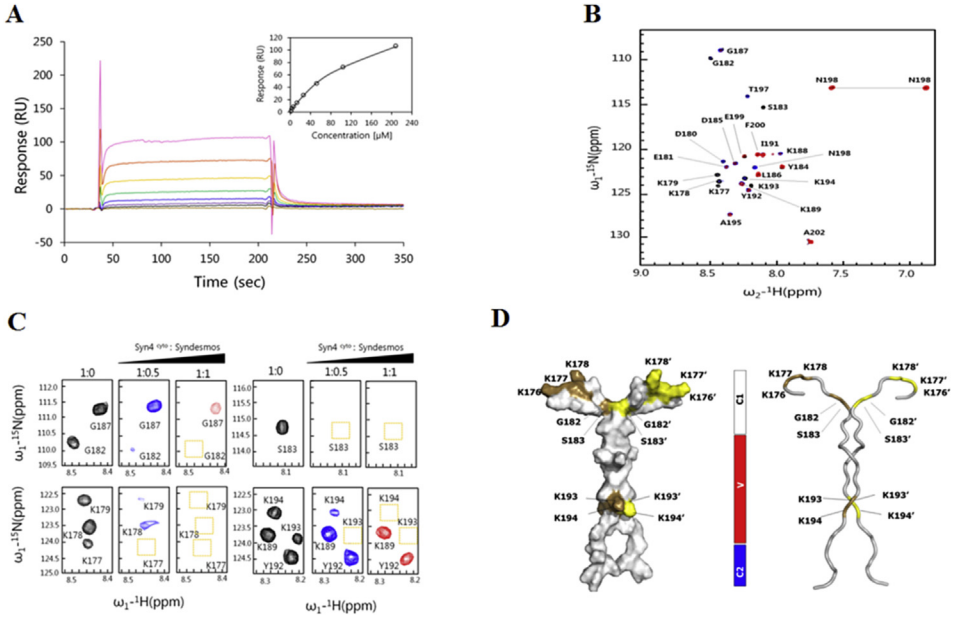

Fig. 4. Molecular interaction between syndesmos and $Syn4^{cyto}$. (A) The syndesmos and $Syn4^{cyto}$ interaction kinetics were determined by surface plasmon resonance (SPR). Biotinylated $Syn4^{cyto}$ peptide was immobilized on a streptavidin-coated SA chip. Syndesmos and $Syn4^{cyto}$ interactions at pH 7.0 were analyzed by injecting different concentrations of syndesmos. Data are shown in the following colors: (——) 1.625 μM, (——) 3.25 μM, (——) 6.50 μM, (——) 13 μM, (——) 26 μM, (——) 52 μM, (——) 104 μM, and (——) 208 μM. RU: response units. (B) Overlay of the two-dimensional $^{1}H-^{15}N$ HSQC spectra of ^{15}N-$Syn4^{cyto}$apo (black) and ^{15}N-$Syn4^{cyto}$ titrated with syndesmos at a 1:1 M ratio (red). $Syn4^{cyto}$ was assigned using 3D-HNCACB, CBCACONH, HNCA, and HNCO. (C) Titration of syndesmos into ^{15}N-$Syn4^{cyto}$ was monitored by ^{15}N NMR, which revealed two binding transitions. The first slow exchange transition corresponds to the canonical syndesmos binding event (1:0, 1:0.5, and 1:1). (D) Surface and ribbon representation of the $Syn4^{cyto}$ dimer. Syndesmos binding residues are represented in orange (chain A) and yellow (chain B). (For interpretation of the colors used in this figure legend, the reader is referred to the web version of this article.)

local structural rearrangement could change the enzyme activity of syndesmos, as well as the loss of the metal-binding amino acids. Regarding syndecan-4 interaction, we identified that several residues, Lys177, Lys178, Lys179, Gly182, and Ser183 in the C1 region, and Lys193 and Lys194 in the V region of syn4^{cyto} bind directly to syndesmos protein. The binding affinity between syndesmos and syn4^{cyto} is relatively weak, K_d = 62 μM. This weak interaction is fundamentally important in promoting rapid on/off switching in signal transduction and transient assembly/disassembly of signaling complexes to regulate critical cellular signaling among several focal adhesion proteins, including paxillin, PKCα, and others, during cell migration and proliferation. Our results will elucidate the structural characteristics of syndesmos and the molecular interaction mechanism of the syndesmos/syn4^{cyto} complex.

Acknowledgments

This work was supported by the Translational Research Center for Protein Function Control (2009-0083522) and the Mid-career Researcher Program (NRF-2013R1A2A2A01068963 to WL) from the Ministry of Future Creation and Science (MFCS) of Korea. Authors thank for technical assistance provided at Beamline 5C (4A) and 7A of the Pohang Light Source and Beamline 1A of the Photon Factory.

Transparency document

Transparency document related to this article can be found online at http://dx.doi.org/10.1016/j.bbrc.2015.06.010.

References

[1] M.J. Bessman, D.N. Frick, S.F. O'Handley, The MutT proteins or "Nudix" hydrolases, a family of versatile, widely distributed, "housecleaning" enzymes, J. Biol. Chem. 271 (1996) 25059–25062.
[2] A.G. McLennan, The nudix hydrolase superfamily, Cell Mol. Life Sci. 63 (2006) 123–143.
[3] M.J. Taylor, B.A. Peculis, Evolutionary conservation supports ancient origin for Nudt16, a nuclear-localized, RNA-binding, RNA-decapping enzyme, Nucleic Acids Res. 36 (2008) 6021–6034.
[4] A.S. Mildvan, Z. Xia, H.F. Azurmendi, V. Sarawat, P.M. Legler, M.A. Massiah, S.B. Gabelli, M.A. Bianchet, L.W. Kang, L.M. Amzel, Structure and mechanisms of nudix hydrolase, Arch. Biochem. Biophys. 433 (2005) 129–143.
[5] T. Dunckley, R. Parker, The DCP2 protein is required for mRNA decapping in Saccharomyces cerevisiae and contains a functional MutT motif, Eur. J. Immunogenet 26 (1999) 423–425.
[6] B.A. Peculis, J.N. Scarsdale, H.T. Wright, Crystal of X29, a Xenopus laevis U8 snoRNA-binding protein with nuclear decapping activity, Acta Crystallogr. D Biol. Cyrstallogr 60 (2004) 1668–1669.
[7] J.N. Scarsdale, B.A. Peculis, H.T. Wright, Crystal structures of U8 snoRNA decapping nudix hydrolase, X29, and its metal and cap complexes, Structure 14 (2006) 331–343.
[8] M. Tucker, R. Parker, Mechanisms and control of mRNA decapping in Saccharomyces cerevisiae, Annu. Rev. Biochem. 69 (2000) 571–595.
[9] T. Ghosh, B. Peterson, N. Tomasevic, B.A. Peculis, *Xenopus* U8 snoRNA binding protein is a conserved nuclear decapping enzyme, Mol. Cell. 13 (2004) 817–828.
[10] P.C. Baciu, S. Saoncella, S.H. Lee, F. Denhez, D. Leuthardt, P.F. Goetinck, Syndesmos, a protein that interacts with the cytoplasmic domain of syndecan-4, mediates cell spreading and actin cytoskeletal organization, Cell Sci. 113 (2000) 315–324.
[11] F. Denhez, S.A. Wilcox-Adelman, P.C. Baciu, S. Saoncella, S. Lee, B. French, W. Neveu, P.F. Goetinck, Syndesmos, a syndecan-4 cytoplasmic domain interactor, binds to the focal adhesion adaptor proteins paxillin and Hic-5, J. Biol. Chem. 277 (2002) 12270–12274.
[12] E. Tkachenko, J.M. Rhodes, M. Simons, Syndecans: new kids on the signaling block, Circ. Res. 96 (2005) 488–500.
[13] S. Tumova, A. Woods, J.R. Couchman, Heparan sulfate proteoglycans on the cell suuface: versatile coordinators of cellular functions, Int. J. Biochem. Cell. Biol. 32 (2000) 269–288.
[14] B.K. Koo, Y.S. Jung, J. Shin, I. Han, E. Mortier, P. Zimmermann, J.R. Whiteford, J.R. Couchman, E.S. Oh, W. Lee, Structural basis of syndecan-4 phosphorylation as a molecular switch to regulate signaling, J. Mol. Biol. 355 (2006) 651–663.
[15] A. Woods, J.R. Couchman, Syndecan-4 and focal adhesion function, Curr. Opin. Cell Biol. 13 (2001) 578–583.
[16] J.J. Grootjans, P. Zimmermann, G. Reekmans, A. Smets, G. Degeest, J. Dürr, G. David, Syntenin, a PDZ protein that binds syndecan cytoplasmic domains, Proc. Natl. Acad. Sci. U. S. A. 94 (1997) 13683–13688.
[17] Y. Gao, M. Li, W. Chen, M. Simons, Synectin, syndecan-4 cytoplasmic domain binding PDZ protein, inhibits cell migration, J. Cell Physiol. 184 (2000) 313–379.
[18] D. Lee, E.S. Oh, A. Woods, J.R. Couchman, W. Lee, Solution structure of a syndecan-4 cytoplasmic domain and its interaction with phosphatidylinositol 4,5-bisphosphate, J. Biol. Chem. 273 (1998) 13022–13029.
[19] E.S. Oh, A. Woods, S.T. Lim, A.W. Theibert, J.R. Couchman, Syndecan-4 proteoglycan cytoplasmic domain and phosphatidylinositol 4,5-bisphosphate coordinately regulate protein kinase C activity, J. Biol. Chem. 273 (1998) 10624–10629.
[20] J.R. Whiteford, S. Ko, W. L, J.R. Couchman, Structural and cell adhesion properties of zebrafish syndecan-4 are shared with higher vertebrates, J. Biol. Chem. 43 (2008) 29322–29330.
[21] Z. Otwinowski, W. Minor, Processing of X-ray diffraction data collected in oscillation mode, Macromol. Crystallogr. Pt A 276 (1997) 307–326.
[22] W.A. Hendrickson, Determination of macromolecular structures from anomalous diffraction of synchrotron radiation, Science 254 (1991) 51–58.
[23] A.L. Morris, M.W. MacArthur, E.G. Hutchinson, J.M. Thornton, Stereochemical quality of protein structure coordinates, Proteins 12 (1992) 345–364.
[24] P.D. Adams, R.W. Grosse-Kunstleve, L.W. Hung, T.R. Ioerger, A.J. McCoy, N.W. Moriarty, R.J. Read, J.C. Sacchettini, N.K. Sauter, T.C. Terwilliger, PHENIX: building new software for automated crystallographic structure determination, Acta Crystallogr. D Biol. Crystallogr. 58 (2002) 1948–1954.
[25] P. Emsley, B. Lohkamp, W.G. Scott, K. Cowtan, Features and development of Coot, Acta Cryst. D 66 (2010) 486–501.
[26] P.D. Adams, P.V. Afonine, G. Bunkóczi, V.B. Chen, I.W. Davis, N. Echols, J.J. Headd, L.W. Hung, G.J. Kapral, R.W. Grosse-Kunstleve, A.J. McCoy, N.W. Moriarty, R. Oeffner, R.J. Read, D.C. Richardson, J.S. Richardson, T.C. Terwilliger, P.H. Zwart, PHENIX: a comprehensive Python-based system for macromolecular structure solution, Acta Cryst. D 66 (2010) 213–221.
[27] E. Krissinel, K. Henrick, Inference of macromolecular assemblies from crystalline state, J. Mol. Biol. 372 (2007) 774–797.
[28] S. Ouyang, X. Song, Y. Wang, H. Ru, N. Shaw, Y. Jiang, F. Niu, Y. Zhu, W. Qiu, K. Parvatiyar, Y. Li, R. Zhang, G. Cheng, Z.J. Liu, Structural analysis of the STING adaptor protein reveals a hydrophobic dimer interface and mode of cyclic di-GMP binding, Immunity 36 (2012) 1073–1086.
[29] J. Stonehouse, R.T. Clowes, G.L. Shaw, J. Keeler, E.D. Laue, Minimisation of sensitivity losses due to the use of gradient pulses in triple-resonance NMR of proteins, J. Biomol. NMR 5 (1995) 226–232.
[30] D.R. Muhandiram, L.E. Kay, Gradient-enhanced triple-resonance threedimensional NMR experiments with improved sensitivity, J. Magn. Reson. 103 (1994) 203–216.
[31] M. Ikura, L.E. Kay, A. Bax, A novel approach for sequential assignment of 1H, 13C, and 15N spectra of proteins: heteronuclear triple-resonance threedimensional NMR spectroscopy application to calmodulin, Biochemistry 29 (1990) 4659–4667.
[32] A. Grzesiek, A. Bax, The origin and removal of artifacts in 3d HCACO spectra of proteins uniformly enriched with 13C, J. Magn. Reson. 102 (1993) 103–106.
[33] F. Delaglio, S. Grzesiek, G.W. Vuister, G. Zhu, J. Pfeifer, A. Bax, NMRPipe: a multidimensional spectral processing system based on UNIX pipes, J. Biomol. NMR 6 (1995) 277–293.